Prescribed Finite-time ESO-based Prescribed Finite-time Control and Its Application to Partial IGC Design

Lei Cui (cui_lei@tju.edu.cn)
Tianjin University https://orcid.org/0000-0002-5238-1357
Nan Jin
Tianjin University

Research Article

Keywords: Prescribed finite-time extended state observer, Peaking value problem, Prescribed finitetime sliding mode controller, Partial integrated guidance and control

Posted Date: June 28th, 2021

DOI: https://doi.org/10.21203/rs.3.rs-643681/v1

Nonlinear Dyn manuscript No.
(will be inserted by the editor)

Prescribed finite-time ESO-based prescribed finite-time control and its application to partial IGC design

Lei Cui · Nan Jin

Received: date / Accepted: date

Abstract This paper proposes a new extended state observer-based sliding mode control strategy with prescribed finite-time convergence. Firstly, a novel prescribed finite-time extended state observer is designed, which estimates the disturbance accurately within a prescribed finite time and effectively solves peaking value problem. Secondly, a new type of second-order prescribed finite-time sliding mode controller is designed to ensure system states converge within a prescribed finite time. Then, the proposed control strategy is applied to the design of partial integrated guidance and control with two-loop controller structure. Finally, the validity of the proposed methodology is verified through numerical simulation.

Keywords Prescribed finite-time extended state observer · Peaking value problem · Prescribed finite-time sliding mode controller · Partial integrated guidance and control

1 Introduction

Over the years, since the property of robustness against bounded disturbance, sliding mode control (SMC) has become the popular tool for the controller design of nonlinear systems [1,2,3,4]. Considering that many conventional sliding mode controllers are designed based on asymptotic stability theory [5], finite-time terminal sliding mode control (TSMC) has been widely developed with the proposed of finite-time theory [6]. By applying the adaptive nonsingular TSMC method, the finite-time convergence of system states was realized in [7]. Considering the 3-D interception of interceptors for hypersonic vehicles, a fast robust control approach using the modified fast TSMC was proposed in [8]. However, in the aforementioned literatures, the settling time of the finite-time control depends on the system initial states, which is usually difficult to be obtained in advance [9]. Especially, for large initial conditions, the settling time may be large and inestimable. As an extension of the finite-time theory, the fixed-time theory was proposed in [10], which ensures the upper-bounded convergence time is a fixed value regardless of initial states [11,12]. Inspired by this attractive feature, TSMC with fixed-time convergence has been widely developed. In [13], a nonsingular fixed-time terminal sliding mode consensus protocol was designed, which accomplishes the fixed-time consensus tracking. A fixed-time TSMC for wheeled mobile robots with bi-limit homogeneous method was designed in [14], the upper bounded convergence time was not given. However, there are still some defects in the existing fixed-time theory [15,16], including that only the upper bound of the convergence time is determined, and the convergence time cannot be arbitrarily assigned by the designer [17]. To address this research problem, in [18,19], a complex time-varying control law was proposed in prescribed finite time, which realizes the convergence of the system in a prescribed finite time. And the settling time is independent of any other design parameters and initial conditions. Similarly, a novel free-will arbitrary-time stable theory was presented as the extension of fixed-time theory in [20]. Therein, a novel controller was designed to stabilize the system in a prescribed time regardless of any system parameters. To the best of authors' knowledge, SMC with prescribed finite-time convergence has seldom been investigated, which motivated us to carry on this

Lei Cui · Nan Jin
the Department of Automation, School of Electrical and Information Engineering, Tianjin University, Tianjin 300072, China
E-mail: cui_lei@tju.edu.cn;nan_jin97@tju.edu.cn

study. Besides, some previous studies have only considered the situation within the prescribed time interval [18,19], which is not conducive to practical application. Hence, it is of great interest to study a new prescribed finite-time convergent SMC theory for nonlinear systems.

Furthermore, as the effective method to deal with disturbance and uncertainty, disturbance/uncertainty estimation and cancelation techniques have captured considerable attention [21], which save control energy significantly in practice. These techniques include unknown input observer (UIO) [22], nonlinear disturbance observer (NDOB) [23], extended state observer (ESO) [14,24,25,26,27]. With the advantages of requiring less information and effectively reducing the tremor problems, ESO technique has been wildly applied in various control systems. ESO is a significant part of active disturbance rejection control [24]. It estimates the so-called "total disturbance" of a system, and the "total disturbance" contains the internal uncertainty, external disturbance and anything that is hard to model or deal with [25]. By incorporating the high-gain approach, a linear ESO was constructed to estimate the uncertain information in the velocity-free large spacecraft system in [26], however it causes the serious peaking value problem. In [25], a nonlinear ESO was designed by introducing piecewise smooth function consisted of linear and fractional power functions, which has the advantage of smaller peaking value. In another aspect, the development for the convergence of ESO is as: asymptotic stability, finite-time stability [27] and fixed-time stability [14]. Recently, with the advent of the arbitrary/prescribed time stability theory [17, 18,19,20], many scholars have begun to study related observers. A new prescribed-time observer with time-varying gains for linear system was proposed in [28], the fixed-time convergence with arbitrary settling time was validated. However, the situation that outside the prescribed time interval was not considered and the observer cannot observe time-varying disturbance or uncertainty. In [29], a new distributed prescribed finite-time observer was designed to observe the disturbance of a strict-feedback nonlinear system on the prescribed finite-time interval. It is to be emphasized that none of the literatures mentioned above addresses the prescribed finite-time stable property of ESO, which motivated us to construct a novel ESO with prescribed finite-time convergence.

Integrated guidance and control (IGC) design can make full use the available information, maximize the missile's maneuverability and improve the terminal performance, which has received wide attention in the past decades [2,30,31]. Thus, a high performance control method is indispensable to accomplish the design. Up to now, plenty of scholars have tried to combine various control methods with partial IGC, such as small gain [32], dynamic surface control [33], linear optimal control [34], backstepping [35], SMC, etc. Note that information of the target acceleration is limited, which is viewed as the disturbance and causes trouble for the controller design. The accuracy requirements may not be met by using conventional techniques. Thus, ESO-based SMC is a good choice.

Inspired by the above discussions, the prescribed finite-time extended state observer-based prescribed finite time sliding mode control (PFTESO-based PFTSMC) strategy will be presented for partial IGC design. The main contributions of this study are summarized as follows. A new type of PFTESO is proposed to estimate and compensate for disturbance, its settling time can be pre-allocated directly and regardless of the initial conditions and any other design parameters. Moreover, the common peaking value problem in the ESO design is effectively reduced. A novel second-order prescribed finite-time sliding mode controller is presented, whose convergence time is independent of the initial conditions and any other design parameters. A new PFTESO-based PFTSMC law is applied to the partial IGC design. Comparing with the adaptive perturbation estimation method, the chattering problem is effectively alleviated without excessively increasing the robust term gain.

The remainder of this paper is organized as follows: Section 2 presents some necessary preliminaries and proposes a novel PFTESO-based PFTSMC law. Section 3 introduces the partial IGC model and reveals the application of proposed control strategy to partial IGC design. Section 4 illustrates the effectiveness. Finally, Section 5 concludes this paper.

Notations In this brief, $\mathbb{R}$ is the set of real numbers and $\mathbb{R}_+$ is the set of positive real numbers, the Euclidean space with dimension p is denoted by $\mathbb{R}^p$. $||\cdot||$ represents Euclidian norm. $\lambda_{\min}(\cdot)$ is the minimum eigenvalue of a matrix $(\cdot)$, $\lambda_{\max}(\cdot)$ is the maximum eigenvalue of a matrix $(\cdot)$. $\lceil x \rfloor^{\alpha} \triangleq |x|^{\alpha}\,\mathrm{sign}(x)$ with $\alpha > 0$, $x \in \mathbb{R}$, and $\mathrm{sign}(x)$ is the sign function, which satisfies $\mathrm{sign}(x) = -1$, if $x < 0$, $\mathrm{sign}(x) = 0$, if $x = 0$, and $\mathrm{sign}(x) = 1$, if $x > 0$. The notation for functions is sometimes simplified, such as, one function $f\big(x(t)\big)$ can be represented as $f(x)$, $f(\cdot)$ or f.

2 Prescribed finite-time extended state observer-based prescribed finite-time sliding mode control

Let's consider a following second-order system

$$\begin{cases} \dot{x}_1 = x_2 \\ \dot{x}_2 = f + bu + \Delta \end{cases} \tag{1}$$

where x_1 and x_2 are the system states, f and $b \neq 0$ are known functions, u represents the control input, Δ denotes the disturbance and is bounded and smooth.

Before designing the control strategy, the following lemma is firstly introduced.

As the basis of this study, a following monotonically increasing function $\Xi(t, t_f) : [0, t_f) \longmapsto \mathbb{R}_+$ is introduced as

$$\Xi(t) = \sec^2\left(\frac{\pi}{2}\frac{t}{t_f}\right), \qquad t \in [0, t_f), \tag{2}$$

where $t_f > 0$ is the prescribed time for meeting the objectives of estimation and control, the function Ξ satisfies the properties that $\Xi(0) = 1$ and $\Xi(t_f) = +\infty$.

Here the qth derivative of $\Xi(t)$ is denoted by $\Xi^{(q)}(t)$ $(q = 0, \ldots, n)$, with $\Xi^{(0)}(t) = \Xi(t)$. By taking the derivatives of Ξ successively, it can be obtained that

$$\Xi^{(q)} = \begin{cases} \sum_{i=1}^{\frac{q+1}{2}} (\frac{\pi}{2t_f})^q a_i^{[q]} m_i, & \text{if q is odd} \\ \sum_{i=1}^{\frac{q+2}{2}} (\frac{\pi}{2t_f})^q a_i^{[q]} m_i, & \text{if q is even} \end{cases}$$

where $m_i = \Xi^i(t) tg^{q-2i+2}(t)$ with $tg(t) = \tan\left(\frac{\pi}{2}\frac{t}{t_f}\right)$; the coefficient $a_i^{[q]}$ satisfies a recursive relationship $a_i^{[q]} = (q - 2i + 3)a_{i-1}^{[q-1]} + 2^i a_i^{[q-1]}$, with $a_0^{[q]} = 0$ and $a_i^{[0]} = 1$.

Lemma 1 *As for a system $g(x(t))$, denote $N \subset \mathbb{R}^n$ as a domain containing the equilibrium point $x = 0$, define $M = [t_0, t_f)$ as the prescribed finite-time interval. Suppose a real-valued continuously differentiable function as $\boldsymbol{V}(\cdot) : \mathbb{R} \times \mathbb{R}^n(N \times M) \to \mathbb{R}_+ \cup \{0\}$, it is a continuous unbounded function and satisfies*

i) $\boldsymbol{V}\big(x(t)\big) = 0 \Leftrightarrow x(t) = 0$;
ii) for any $x(t) \neq 0$, there exists $k > 0$ such that

$$\dot{\boldsymbol{V}}\big(x(t)\big) \leq -k\Xi(t)\boldsymbol{V}\big(x(t)\big)$$

then the function $\boldsymbol{V}(t)$ satisfies $\lim_{t \to t_f^-} \boldsymbol{V}(t) = 0$.

Proof It is known that in time interval M, the value of function Ξ is greater than 0, thus, $\dot{\boldsymbol{V}} \leq 0$ and the system state is convergent. Integrating it yields

$$\begin{aligned} \boldsymbol{V}(t) &\leq \exp^{-k\int_{t_0}^{t} \Xi(\tau)d\tau} \boldsymbol{V}(t_0) \\ &\leq \exp^{-\frac{2kt_f}{\pi} Tg(t)} \boldsymbol{V}(t_0) \end{aligned}$$

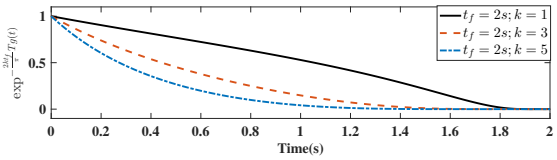

Fig. 1 The curve of the function $\exp^{-\frac{2kt_f}{\pi}Tg(t)}$

where $Tg(t) = \big(tg(t) - tg(t_0)\big)$, and t_0 is the initial time. The function $\exp^{-\frac{2kt_f}{\pi}Tg(t)}$ satisfies the properties that $\exp^{-\frac{2kt_f}{\pi}Tg(t_0)} = 1$ and $\exp^{-\frac{2kt_f}{\pi}Tg(t_f)} = 0$, which can be found in Fig. 1. Because the initial system state $x(t_0)$ and $\boldsymbol{V}(t_0)$ are positive bounded real numbers, then it is obtained that $\lim_{t \to t_f^-} \boldsymbol{V}(t) = 0$. The proof of Lemma 1 is completed.

2.1 PFTESO design

This subsection is concerned with the PFTESO design for estimating the disturbance in system (1). In [7], the disturbance was addressed by using an adaptive method. However, the initial estimation of disturbance needs to be large enough, which results in overestimation of switch control input, wastes the energy of control and causes negative chattering problem [36]. The disturbance can be estimated by the proposed novel PFTESO. In this way, the chattering problem is alleviated and control power is minimized.

Firstly, the disturbance Δ is extended by x_3. Consequently, the extended state system is described by

$$\begin{cases} \dot{x}_1 = x_2 \\ \dot{x}_2 = f + bu + \Delta \\ \dot{x}_3 = \dot{\Delta} \end{cases} \tag{3}$$

Assumption 1 [25] $\dot{\Delta}$ is bounded and smooth, i.e., $|\dot{\Delta}| \leq \dot{\Delta}_{\max}$ with $\dot{\Delta}_{\max}$ being a constant.

The objective is to design a PFTESO for estimating disturbance within a prescribed finite time. The settling time can be prescribed *a priori* regardless of other design parameters and system initial conditions. In the prescribed time interval, the observer error can be guaranteed to converge to the origin by introducing the monotone increasing function $\overline{\Xi}$. Then, the proposed ESO switches to the form of Levant's robust exact differentiator in [37], so that the observation error can be maintained at the origin in the later time. Based on such a design idea, the structure of PFTESO for the

extended state system (3) can be constructed as

$$\begin{cases} \varphi_1 = x_1 - \hat{x}_1 \\ \dot{\hat{x}}_1 = \hat{x}_2 + \mathcal{T}\zeta\overline{\Xi}l_1\varphi_1 + (1-\mathcal{T})k_1\Gamma^{\frac{1}{3}}\lceil\varphi_1\rfloor^{\frac{2}{3}} \\ \dot{\hat{x}}_2 = f + bu + \hat{\Delta} + \mathcal{T}\zeta^2\overline{\Xi}^2 l_2\varphi_1 + (1-\mathcal{T})k_2\Gamma^{\frac{2}{3}}\lceil\varphi_1\rfloor^{\frac{1}{3}} \\ \dot{\hat{\Delta}} = \mathcal{T}\zeta^3\overline{\Xi}^3 l_3\varphi_1 + (1-\mathcal{T})k_3\Gamma\lceil\varphi_1\rfloor^0 \end{cases} \tag{4}$$

where $\overline{\Xi} = \sec^2\left(\frac{\pi}{2}\frac{t}{\overline{t}_f}\right), t \in [0, \overline{t}_f)$, and $\overline{t}_f$ is the prescribed convergence time for the PFTESO; ζ and $l_{1,2,3}$ are the tunable parameters; $k_3 > \Gamma \geq \dot{\Delta}_{\max}$, $k_1 = 3.34k_3^{\frac{1}{3}}$ and $k_2 = 5.3k_3^{\frac{2}{3}}$; $\mathcal{T}$ is the time switching function of the PFTESO, which satisfies

$$\mathcal{T} = \begin{cases} 1, t \in [0, \overline{t}_f) \\ 0, t \in [\overline{t}_f, +\infty) \end{cases}$$

Then the error system can be described by

$$\begin{cases} \dot{\varphi}_1 = \varphi_2 - \mathcal{T}\zeta\overline{\Xi}l_1\varphi_1 - (1-\mathcal{T})k_1\Gamma^{\frac{1}{3}}\lceil\varphi_1\rfloor^{\frac{2}{3}} \\ \dot{\varphi}_2 = \varphi_3 - \mathcal{T}\zeta^2\overline{\Xi}^2 l_2\varphi_1 - (1-\mathcal{T})k_2\Gamma^{\frac{2}{3}}\lceil\varphi_1\rfloor^{\frac{1}{3}} \\ \dot{\varphi}_3 = \dot{\Delta} - \mathcal{T}\zeta^3\overline{\Xi}^3 l_3\varphi_1 - (1-\mathcal{T})k_3\Gamma\lceil\varphi_1\rfloor^0 \end{cases} \tag{5}$$

where $\varphi_2 = x_2 - \hat{x}_2$ and $\varphi_3 = x_3 - \hat{\Delta}$.

Theorem 1 *For system (1) with the designed PFTESO (4), the states of error system (5) can achieve convergence within the prescribed time $\overline{t}_f$, and they will be maintained at the origin within the time interval $\overline{D} : t \in [\overline{t}_f, \infty)$.*

Proof 1) Consider the situation within the time interval $t \in [0, \overline{t}_f)$ firstly, the error system (5) is rearranged as

$$\begin{cases} \dot{\varphi}_1 = \varphi_2 - \zeta\overline{\Xi}l_1\varphi_1 \\ \dot{\varphi}_2 = \varphi_3 - \zeta^2\overline{\Xi}^2 l_2\varphi_1 \\ \dot{\varphi}_3 = \dot{\Delta} - \zeta^3\overline{\Xi}^3 l_3\varphi_1 \end{cases}$$

which can be rewritten more compactly as

$$\dot{\boldsymbol{\varphi}} = A\boldsymbol{\varphi} - \Psi LC\boldsymbol{\varphi} + W \tag{6}$$

where $\boldsymbol{\varphi} = [\varphi_1, \varphi_2, \varphi_3]^T$, $\Psi = \mathrm{diag}\{\zeta\overline{\Xi}, \zeta^2\overline{\Xi}^2, \zeta^3\overline{\Xi}^3\}$, $L = [l_1, l_2, l_3]^T$, $C = [1, 0, 0]$, $W = [0, 0, \dot{\Delta}]^T$, and the matrix A satisfies

$$A = \begin{bmatrix} 0 & 1 & 0 \\ 0 & 0 & 1 \\ 0 & 0 & 0 \end{bmatrix}.$$

Then, the following state transformation is introduced

$$\widetilde{\boldsymbol{\varphi}} = \widetilde{\Psi}\boldsymbol{\varphi} \tag{7}$$

where $\widetilde{\Psi}$ is a transformation matrix denoted as $\widetilde{\Psi} = \mathrm{diag}\{\zeta^3\overline{\Xi}^3, \zeta^2\overline{\Xi}^2, \zeta\overline{\Xi}\}$. Since the special properties of $\overline{\Xi}$, it's easy to know $\lim_{t\to\overline{t}_f}\|\widetilde{\Psi}\| = +\infty$. In addition, differentiating (7) and substituting (6) into it yields

$$\begin{aligned} \dot{\widetilde{\boldsymbol{\varphi}}} &= \dot{\widetilde{\Psi}}\boldsymbol{\varphi} + \widetilde{\Psi}\dot{\boldsymbol{\varphi}} \\ &= \rho\overline{\Xi}D\widetilde{\boldsymbol{\varphi}} + \overline{\Xi}\zeta(A - LC)\widetilde{\boldsymbol{\varphi}} + \widetilde{\Psi}W \end{aligned}$$

where $D = \mathrm{diag}\{3, 2, 1\}$, $\rho = \frac{\pi}{2\overline{t}_f}\sin(\frac{\pi}{\overline{t}_f}t) \leq \frac{\pi}{2\overline{t}_f}$.

Consider a Lyapunov function candidate as

$$V_{\widetilde{\boldsymbol{\varphi}}} = \widetilde{\boldsymbol{\varphi}}^T P\widetilde{\boldsymbol{\varphi}}$$

where P is a positive definite symmetric matrix. The matrices P, A, L and C satisfy the linear matrix inequalities in Lemma 5 of Ref. [29], it yields

$$\begin{aligned} (A - LC)^T P + P(A - LC) &\leq A + A^T - \gamma I_n \\ \underline{\nu} I_n \leq PD + DP &\leq \overline{\nu} I_n \end{aligned} \tag{8}$$

where γ can be any constant, and $\underline{\nu}$ and $\overline{\nu}$ are the positive constants.

According to Rayleigh's inequalities, it is rearranged as

$$\lambda_{\min}(P)||\widetilde{\boldsymbol{\varphi}}||^2 \leq V_{\widetilde{\boldsymbol{\varphi}}} \leq \lambda_{\max}(P)||\widetilde{\boldsymbol{\varphi}}||^2$$

The time derivative of $V_{\widetilde{\boldsymbol{\varphi}}}$ along the trajectory of (7) can be calculated as

$$\begin{aligned} \dot{V}_{\widetilde{\boldsymbol{\varphi}}} =& \dot{\widetilde{\boldsymbol{\varphi}}}^T P\widetilde{\boldsymbol{\varphi}} + \widetilde{\boldsymbol{\varphi}}^T P\dot{\widetilde{\boldsymbol{\varphi}}} \\ =& \rho\overline{\Xi}\widetilde{\boldsymbol{\varphi}}^T(D^T P + PD)\widetilde{\boldsymbol{\varphi}} \\ &+ \overline{\Xi}\zeta\widetilde{\boldsymbol{\varphi}}^T[(A - LC)^T P + P(A - LC)]\widetilde{\boldsymbol{\varphi}} \\ &+ W^T\widetilde{\Psi}^T P\widetilde{\boldsymbol{\varphi}} + \widetilde{\boldsymbol{\varphi}}^T P\widetilde{\Psi}W \end{aligned} \tag{9}$$

According to (8), the second term of right-hand side in (9) satisfies $\overline{\Xi}\zeta\widetilde{\boldsymbol{\varphi}}^T[(A - LC)^T P + P(A - LC)]\widetilde{\boldsymbol{\varphi}} \leq \overline{\Xi}\zeta\widetilde{\boldsymbol{\varphi}}^T(A^T + A - \gamma I_n)\widetilde{\boldsymbol{\varphi}}$, then it can be obtained that

$$\begin{aligned} \dot{V}_{\widetilde{\boldsymbol{\varphi}}} \leq& \rho\overline{\Xi}\widetilde{\boldsymbol{\varphi}}^T(DP + PD)\widetilde{\boldsymbol{\varphi}} + W^T\widetilde{\Psi}^T P\widetilde{\boldsymbol{\varphi}} + \widetilde{\boldsymbol{\varphi}}^T P\widetilde{\Psi}W \\ &+ \overline{\Xi}\zeta\widetilde{\boldsymbol{\varphi}}^T(A^T + A - \gamma I_n)\widetilde{\boldsymbol{\varphi}} \\ \leq& \overline{\nu}\rho\overline{\Xi}\|\widetilde{\boldsymbol{\varphi}}\|^2 + 2\overline{\Xi}\zeta\|A\|\|\widetilde{\boldsymbol{\varphi}}\|^2 - \overline{\Xi}\zeta\gamma\|\widetilde{\boldsymbol{\varphi}}\|^2 \\ &+ \overline{\Xi}\dot{\Delta}\big((p_3 + p_7)\|\widetilde{\varphi}_1\| + (p_6 + p_8)\|\widetilde{\varphi}_2\| + 2p_9\|\widetilde{\varphi}_3\|\big) \\ \leq& \overline{\nu}\rho\overline{\Xi}\|\widetilde{\boldsymbol{\varphi}}\|^2 + 2\overline{\Xi}\zeta\|A\|\|\widetilde{\boldsymbol{\varphi}}\|^2 - \overline{\Xi}\zeta\gamma\|\widetilde{\boldsymbol{\varphi}}\|^2 \\ &+ 6\overline{p}\overline{\Xi}\|\dot{\Delta}\|\|\widetilde{\boldsymbol{\varphi}}\| \end{aligned}$$

where p_i $(i = 1, \cdots, 9)$ are the members of the matrix $P = \begin{bmatrix} p_1 & p_2 & p_3 \\ p_4 & p_5 & p_6 \\ p_7 & p_8 & p_9 \end{bmatrix}$, and $\overline{p} = \max\{|p_3|, |p_6|, |p_7|, |p_8|, |p_9|\}$ is a bounded number. Then, it can be obtained by using Young's inequality

$$6\overline{p}\overline{\Xi}\|\dot{\Delta}\|\|\widetilde{\boldsymbol{\varphi}}\| \leq \epsilon\overline{\Xi}\|\widetilde{\boldsymbol{\varphi}}\|^2 + \frac{\overline{\Xi}}{\epsilon}\left(3\overline{p}\|\dot{\Delta}\|\right)^2$$

where $\epsilon > 0$.

Choosing $\zeta \geq \frac{\overline{\nu}\pi}{2\overline{t}_f} + \epsilon$, $\gamma \geq 1 + 2\|A\|$ and defining $\varrho = \zeta(\gamma - 2\|A\| - 1) > 0$, one can obtain

$$\begin{aligned}\dot{V}_{\widetilde{\boldsymbol{\varphi}}} &\leq -\varrho\overline{\Xi}\|\widetilde{\boldsymbol{\varphi}}\|^2 + \frac{\overline{\Xi}}{\epsilon}\left(3\overline{p}\|\dot{\Delta}\|\right)^2 \\ &\leq -\vartheta\overline{\Xi}V_{\widetilde{\boldsymbol{\varphi}}} + \frac{\overline{\Xi}}{\epsilon}\left(3\overline{p}\|\dot{\Delta}\|\right)^2\end{aligned}$$

where $\vartheta = \frac{\varrho}{\lambda_{\max}(P)} > 0$.

According to the solution of inhomogeneous differential equation, it yields

$$\begin{aligned}&V_{\widetilde{\boldsymbol{\varphi}}}(t) \\ \leq& \exp^{-\vartheta\int_{t_0}^{t}\overline{\Xi}(\tau)\mathrm{d}\tau} V_{\widetilde{\boldsymbol{\varphi}}}(t_0) \\ &+ \frac{9\overline{p}^2}{\epsilon}\int_{t_0}^{t}\exp^{-\vartheta\int_{\tau}^{t}\overline{\Xi}(s)\mathrm{d}s}\dot{\Delta}(\tau)^2\overline{\Xi}(\tau)\mathrm{d}\tau \\ \leq& \exp^{-\frac{2\vartheta\overline{t}_f}{\pi}Tg(t)} V_{\widetilde{\boldsymbol{\varphi}}}(t_0) \\ &+ \frac{\mathcal{W}}{\epsilon}\int_{t_0}^{t}\exp^{\vartheta\left(-\int_{t_0}^{t}\overline{\Xi}(s)\mathrm{d}s+\int_{t_0}^{\tau}\overline{\Xi}(s)\mathrm{d}s\right)}\overline{\Xi}(\tau)\mathrm{d}\tau \\ =& \exp^{-\frac{2\vartheta\overline{t}_f}{\pi}Tg(t)} V_{\widetilde{\boldsymbol{\varphi}}}(t_0) \\ &+ \frac{\mathcal{W}}{\epsilon}\exp^{-\vartheta\int_{t_0}^{t}\overline{\Xi}(s)\mathrm{d}s}\int_{t_0}^{t}\exp^{\vartheta\int_{t_0}^{\tau}\overline{\Xi}(s)\mathrm{d}s}\mathrm{d}\left(\int_{t_0}^{\tau}\overline{\Xi}(s)\mathrm{d}s\right) \\ =& \exp^{-\frac{2\vartheta\overline{t}_f}{\pi}Tg(t)} V_{\widetilde{\boldsymbol{\varphi}}}(t_0) \\ &+ \frac{\mathcal{W}}{\vartheta\epsilon}\exp^{-\vartheta\int_{t_0}^{t}\overline{\Xi}(s)\mathrm{d}s}\exp^{\vartheta\int_{t_0}^{\tau}\overline{\Xi}(s)\mathrm{d}s}\Big|_{t_0}^{t} \\ =& \exp^{-\frac{2\vartheta\overline{t}_f}{\pi}Tg(t)} V_{\widetilde{\boldsymbol{\varphi}}}(t_0) \\ &+ \frac{\mathcal{W}}{\vartheta\epsilon}\exp^{-\vartheta\int_{t_0}^{t}\overline{\Xi}(s)\mathrm{d}s}\left(\exp^{\vartheta\int_{t_0}^{t}\overline{\Xi}(s)\mathrm{d}s} - 1\right) \\ =& \exp^{-\frac{2\vartheta\overline{t}_f}{\pi}Tg(t)} V_{\widetilde{\boldsymbol{\varphi}}}(t_0) + \frac{\mathcal{W}}{\vartheta\epsilon}\left(1 - \exp^{-\vartheta\int_{t_0}^{t}\overline{\Xi}(s)\mathrm{d}s}\right) \\ \leq& \exp^{-\frac{2\vartheta\overline{t}_f}{\pi}Tg(t)} V_{\widetilde{\boldsymbol{\varphi}}}(t_0) + \frac{\mathcal{W}}{\vartheta\epsilon}\end{aligned}$$

where $\mathcal{W} = 9\overline{p}^2\dot{\Delta}_{\max}^2$, and it implies that $V_{\widetilde{\boldsymbol{\varphi}}}(t)$ and $\widetilde{\boldsymbol{\varphi}}(t)$ are bounded in the time interval $t \in [0, \overline{t}_f)$. Further,

$$\begin{aligned}\|\boldsymbol{\varphi}(t)\|^2 &= \|\widetilde{\Psi}^{-1}\widetilde{\boldsymbol{\varphi}}\|^2 \\ &\leq \|\widetilde{\Psi}^{-1}\|^2\|\widetilde{\boldsymbol{\varphi}}\|^2 \\ &\leq \frac{\|\widetilde{\Psi}^{-1}\|^2}{\lambda_{\min}(P)}\left(\underbrace{\exp^{-\frac{2\vartheta\overline{t}_f}{\pi}Tg(t)} V_{\widetilde{\boldsymbol{\varphi}}}(t_0) + \frac{\mathcal{W}}{\vartheta\epsilon}}_{\mathcal{F}}\right)\end{aligned} \tag{10}$$

where $\mathcal{F}$ is bounded real number in the time interval $t \in [0, \overline{t}_f)$, $\widetilde{\Psi}$ satisfies $\|\widetilde{\Psi}(0)^{-1}\| = 1$ and $\lim_{t\to\overline{t}_f}\|\widetilde{\Psi}(t)^{-1}\| = 0$. Thus, it's easy to obtain that $\lim_{t\to\overline{t}_f}\|\boldsymbol{\varphi}(t)\| = 0$, which implies that the estimate errors converge to 0 in the prescribed finite time.

2) Then, consider the situation within the time interval $t \in [\overline{t}_f, \infty)$, and the PFTESO for the extended state system (3) can be rewritten as

$$\begin{cases}\varphi_1 = x_1 - \hat{x}_1 \\ \dot{\hat{x}}_1 = \hat{x}_2 + k_1\Gamma^{\frac{1}{3}}\lceil\varphi_1\rfloor^{\frac{2}{3}} \\ \dot{\hat{x}}_2 = f + bu + \hat{\Delta} + k_2\Gamma^{\frac{2}{3}}\lceil\varphi_1\rfloor^{\frac{1}{3}} \\ \dot{\Delta} = k_3\Gamma\lceil\varphi_1\rfloor^0\end{cases}$$

which is the form of Levant's third-order robust exact differentiator in [37]. Let's rearrange the error system (5) in the following form

$$\begin{cases}\dot{\varphi}_1 = \varphi_2 - k_1\Gamma^{\frac{1}{3}}\lceil\varphi_1\rfloor^{\frac{2}{3}} \\ \dot{\varphi}_2 = \varphi_3 - k_2\Gamma^{\frac{2}{3}}\lceil\varphi_1\rfloor^{\frac{1}{3}} \\ \dot{\varphi}_3 = \dot{\Delta} - k_3\Gamma\lceil\varphi_1\rfloor^0\end{cases}$$

According to the Theorem 1 in Cruz-Zavala and Moreno's paper [37], for a given $p \geq 2n - 1 = 5$, there exists a valid set of gain parameters $k_i (i = 1, 2, 3)$ such that a suitable positive definite function V_Υ can be found, which satisfies its differential inequality for a positive κ

$$\dot{V}_\Upsilon \leq -\kappa V_\Upsilon^{\frac{p-1}{p}}$$

where the Lyapunov function candidate is

$$V_\Upsilon = \sum_{j=1}^{2}\alpha_j\Upsilon_j(\upsilon_j, \upsilon_{j+1}) + \alpha_3\frac{1}{p}|\upsilon_3|^p$$

with arbitrary $\alpha_{1,2,3} > 0$, $r_i = 4 - i (i = 1, 2, 3)$ and

$$\upsilon_1 = \frac{\varphi_1}{\Gamma}, \upsilon_2 = \frac{\varphi_2}{k_1\Gamma}, \upsilon_3 = \frac{\varphi_3}{k_2\Gamma}$$

$$\begin{aligned}\Upsilon_i(\upsilon_i, \upsilon_{i+1}) =& \frac{r_i}{p}|\upsilon_i|^{\frac{p}{r_i}} - \upsilon_i\lceil\upsilon_{i+1}\rfloor^{\frac{p-r_i}{r_{i+1}}} \\ &+ \left(\frac{p - r_i}{p}\right)|\upsilon_{i+1}|^{\frac{p}{r_{i+1}}}\end{aligned}$$

Through the above discussion and $\lim_{t\to\overline{t}_f}\|\boldsymbol{\varphi}\| = 0$, it's easy to obtain that the newly defined Lyapunov function candidate satisfies $\lim_{t\to\overline{t}_f} V_\Upsilon = 0$. According to the Proposition 1 in [37], if the parameters are chosen as $k_3 > \Gamma \geq \dot{\Delta}_{\max}$, $k_1 = 3.34k_3^{\frac{1}{3}}$ and $k_2 = 5.3k_3^{\frac{2}{3}}$, then the derivative of V_Υ satisfies $\dot{V}_\Upsilon \leq -\kappa V_\Upsilon^{\frac{p-1}{p}} \leq 0$. So that the Lyapunov function candidate V_Υ is going to remain on $V_\Upsilon = 0$ in the time interval $\overline{D}$. In other words, $\|\boldsymbol{\varphi}\| \equiv 0$ is maintained in the rest of the time. This completes the proof.

Remark 1 Compared with the existing linear ESO [26], nonlinear ESO [25], finite-time ESO [27] or fixed-time ESO [14], the estimate errors' convergence time of the proposed PFTESO is a prescribed finite time, which can meet the control requirement better. Besides, plenty of previous methods for ESO design can only ensure

that the observation error converging to the neighborhood of the origin. The observation accuracy needs to be improved by high gain [26], thereby peaking value problem appears. In this study, the monotone increasing function $\overline{\Xi}$ is introduced in the initial stage, and the initial gains $l_{1,2,3}$ can be set small to significantly reduce the peaking value problem. The effectiveness of this part will be verified in the simulation part of Subsection 4.1.

Remark 2 On one hand, the proposed PFTESO considers not only the observations within the prescribed time interval but also the case outside the time interval. By switching to the form of Levant's robust exact differentiator [37], the observation error can be maintained at the origin. Therefore, compared to the existing prescribed-time observer [28], the proposed PFTESO is more suitable for practical implementation. On the other hand, the proposed PFTESO can realize the observation of the extended system state, which can be used to estimate the total disturbance in the system. This is another advantage over the prescribed-time observer in [28].

2.2 PFTESO-based PFTSMC law design

In this subsection, a PFTSMC method is designed to guarantee that the states of system (1) converge within a prescribed finite time, and could be maintained at the origin after the prescribed time. For the existing disturbance, the proposed PFTESO is used to estimate it for compensating in the controller.

For system (1), a prescribed finite-time convergent sliding mode controller is constructed as

$$u=\begin{cases}-b^{-1}\big(\hat{\Delta}+\kappa_1\Xi_2 x_2+\kappa_1\Xi_2^{(1)}x_1+\kappa_2\Xi_1 s+f+l\,\mathrm{sign}(s)\big),\\ t\in[0,t_{f1})\\ -b^{-1}\big(\hat{\Delta}+\kappa_1\Xi_2 x_2+\kappa_1\Xi_2^{(1)}x_1+k_1 s+f+l\,\mathrm{sign}(s)\big),\\ t\in[t_{f1},t_{f2})\\ -b^{-1}\big(\hat{\Delta}+k_1 s+k_2 x_2+f+l\,\mathrm{sign}(s)\big),\\ t\in[t_{f2},+\infty)\end{cases}\tag{11}$$

And the prescribed finite-time sliding mode surface is described as follow:

$$s=\begin{cases}x_2+\kappa_1\Xi_2 x_1, & t\in[0,t_{f2})\\ x_2+k_2 x_1, & t\in[t_{f2},+\infty)\end{cases}\tag{12}$$

where $\kappa_1>\Psi$, $\kappa_2>\frac{\pi}{2t_{f1}}$, $k_{1,2}>0$, $l>0$ are the tunable parameters and $\Psi=\max\{\frac{\pi}{t_{f2}},\frac{\pi}{2t_{f2}}\big(1+\cot(\frac{\pi t_{f1}}{2t_{f2}})\big)\}$; $\Xi_1=\sec^2\left(\frac{\pi}{2}\frac{t}{t_{f1}}\right)$ and $\Xi_2=\sec^2\left(\frac{\pi}{2}\frac{t}{t_{f2}}\right)$ are the time varying gains, t_{f1}, t_{f2} are the prescribed convergence time for the sliding mode surface and system states, respectively. The prescribed convergence time satisfies $\overline{t}_f<t_{f1}<t_{f2}$.

Theorem 2 *For system (1), if the PFTSMC is designed as (11) with the prescribed finite-time sliding manifold (12). Then the following two points can be obtained as:*

1) *system states x_1, x_2 can reach the sliding manifold s in the prescribed time t_{f1}, and the sliding manifold s will be maintained at the origin within the time interval $D_1: t\in[t_{f1},\infty)$;*
2) *system states x_1, x_2 will converge to the origin in the prescribed time t_{f2}, and they will be maintained at the origin within the time interval $D_2: t\in[t_{f2},\infty)$.*

Proof 1) Consider the reaching phase $\big(s\neq 0; t\in[0,t_{f1})\big)$, differentiating (12) along dynamics (1) and substituting the law (11) into it yields

$$\begin{aligned}\dot{s}&=\Delta-\hat{\Delta}-\kappa_2\Xi_1 s-l\,\mathrm{sign}(s)\\&=\varphi_3-\kappa_2\Xi_1 s-l\,\mathrm{sign}(s)\end{aligned}$$

Consider a Lyapunov function candidate as $V_1=s^2/2$, it can be obtained that $\dot{V}_1\leq-2\kappa_2\Xi_1 V_1-(l-|\varphi_3|)V_1^{\frac{1}{2}}$. According to (10), in the time interval $t\in[0,\overline{t}_f)$, $\|\boldsymbol{\varphi}\|^2\leq\frac{\|\widetilde{\Psi}^{-1}\|^2}{\lambda_{\min}(P)}\mathcal{F}$ is bounded. Besides, since $\overline{t}_f\leq t_{f1}$, we know that the boundedness of φ_3 can be guaranteed in the time interval $t\in[0,t_{f1})$, and $l-|\varphi_3|$ is a bounded coefficient. Thus, the value on the right hand of this inequality is finite for any finite time. We can come to the conclusion that V_1 and s can't escape to infinite before $\boldsymbol{\varphi}$ converges to the origin in the prescribed time $\overline{t}_f$. Once the estimation error satisfies $|\varphi_3|\leq l$, it is obtained that $\dot{V}_1\leq-2\kappa_2\Xi_1 V_1$. According to Lemma 1, the system states converge to the sliding surface in the prescribed time t_{f1}.

Considering the special properties of function Ξ_1, the boundedness of the term $\kappa_1\Xi_1 s$ of the control input is discussed within the specified time t_{f1}. Another Lyapunov function candidate is considered as $V_2=\frac{1}{2}(\Xi_1 s_1)^2$, in the time interval $t\in[\overline{t}_f,t_{f1})$, it yields

$$\begin{aligned}\dot{V}_2&=(\Xi_1 s)(\Xi_1\dot{s}_1+\Xi_1^{(1)}s)\\&\leq(\Xi_1 s)^2\big(-\kappa_2\Xi_1+\frac{\pi}{t_{f1}}tg_1(t)\big)\\&=-L\Xi_1(\Xi_1 s)^2\\&=-2L\Xi_1 V_2\end{aligned}$$

where $L=\kappa_2-\frac{\pi}{2t_{f1}}\sin(\frac{\pi}{t_{f1}}t)>0$, $\Xi_1^{(1)}=\frac{\pi}{t_{f1}}tg_1(t)\Xi_1$ and $tg_1(t)=\frac{1}{2}\Xi_1\sin(\frac{\pi t}{t_{f1}})$ have been used. According to Lemma 1, it is obtained that $\lim_{t\to t_{f1}^-}V_2=0$, which means $\lim_{t\to t_{f1}^-}\Xi_1 s=0$. It is equivalent to the term $\kappa_1\Xi_1 s$ will eventually converge to 0 within the specified time t_{f1}, which implies that the control input is bounded over $t\in[0,t_{f1})$ with the control law (11).

In the time interval $t \in [t_{f1}, t_{f2})$, the control law (11) switches to the following form

$$u = -b^{-1}\big(\hat{\Delta} + k_1 s + \kappa_1 \Xi_2 x_2 + \kappa_1 \Xi_2^{(1)} x_1 + f + l\,\mathrm{sign}(s)\big)$$

where the term $\kappa_2 \Xi_1 s$ switches to $k_1 s$. Obviously, it's easy to know that $\lim_{t\to t_{f1}^-} \kappa_2 \Xi_1 s = \lim_{t\to t_{f1}^+} k_1 s = 0$. And it can be obtained that

$$V_1(t_{f1}) = \lim_{t\to t_{f1}^-} V_1(t) = 0$$

For the time interval $D_1 : t \in [t_{f1}, \infty)$, the Lyapunov function candidate is also chosen as $V_1 = s^2/2$, we readily obtain:

$$\dot{V}_1 = -k_1 s^2 - l|s| \le 0, \qquad t \in [t_{f1}, \infty)$$

and it yields

$$0 \le V_1(t) \le V_1(t_{f1}) = 0, \qquad t \in [t_{f1}, \infty)$$

which means that $s \equiv 0$ is kept over the time interval D_1. This completes the proof of point 1).

2) In the sliding phase $\big(s \equiv 0, t \in [t_{f1}, t_{f2})\big)$, it is firstly obtained that

$$s \equiv 0 \Rightarrow \dot{x}_1 = x_2 = -\kappa_1 \Xi_2 x_1$$

Then consider another Lyapunov function candidate as $V_3 = \frac{1}{2}x_1^2 + \frac{1}{2}x_2^2$, it yields

$$\begin{aligned}
\dot{V}_3 &= x_1\dot{x}_1 + x_2\dot{x}_2 \\
&= -\kappa_1 \Xi_2 x_1^2 + x_2(-\kappa_1 \Xi_2 x_2 - \kappa_1 \Xi_2^{(1)} x_1) \\
&= -\kappa_1 \Xi_2 x_1^2 + x_2(-\kappa_1 \Xi_2 x_2 + \frac{\Xi_2^{(1)}}{\Xi_2} x_2) \\
&= -\kappa_1 \Xi_2 x_1^2 + x_2\big(-\kappa_1 \Xi_2 x_2 + \frac{\pi}{t_{f2}} t g_2(t) x_2\big) \\
&\le -\kappa_1 \Xi_2 x_1^2 - L^{'} \Xi_2 x_2^2 \\
&\le -2L^{'} \Xi_2 V_3
\end{aligned}$$

where $L^{'} = \kappa_1 - \frac{\pi}{2t_{f2}} \sin(\frac{\pi}{t_{f2}} t) > 0$, $\Xi_2^{(1)} = \frac{\pi}{t_{f2}} t g_2(t) \Xi_2$, and $t g_2(t) = \frac{1}{2}\Xi_2 \sin(\frac{\pi t}{t_{f2}})$ have been used. According to Lemma 1, it can be obtained that $\lim_{t\to t_{f2}^-} V_3 = 0$, which is equivalent to $\lim_{t\to t_{f2}^-} x_{1,2} = 0$. Similarly, considering the special properties of function Ξ_2, the boundedness of the terms $\kappa_1 \Xi_2 x_2$ and $\kappa_1 \Xi_2^{(1)} x_1$ of the control input is discussed within the time interval $t \in [t_{f1}, t_{f2})$. Another Lyapunov function candidate is chosen as $V_4 = \frac{1}{2}(\Xi_2 x_2)^2 + \frac{1}{2}(\Xi_2^{(1)} x_1)^2$, it yields

$$\begin{aligned}
&\dot{V}_4 \\
=&(\Xi_2 x_2)\big(\Xi_2(-\kappa_1 \Xi_2 x_2 - \kappa_1 \Xi_2^{(1)} x_1) + \Xi_2^{(1)} x_2\big) \\
&+ (\Xi_2^{(1)} x_1)(\Xi_2^{(1)} x_2 + \Xi_2^{(2)} x_1) \\
=&-(\Xi_2 x_2)^2\big(\kappa_1 \Xi_2 - \frac{\pi}{2t_{f2}} \sin(\frac{\pi t}{t_{f2}}) \Xi_2 - \frac{\pi}{2t_{f2}} \sin(\frac{\pi t}{t_{f2}}) \Xi_2\big) \\
&-(\Xi_2^{(1)} x_1)^2\big(\Xi_2 \kappa_1 - \frac{\pi}{2t_{f2}}(2 t g_2(t) + \frac{\Xi_2}{t g_2(t)})\big) \\
\le&-L^{''} \Xi_2 (\Xi_2 x_2)^2 - L^{'''} \Xi_2 (\Xi_2^{(1)} x_1)^2 \\
\le&-2\overline{L} \Xi_2 V_4
\end{aligned}$$

where $L^{''} = \kappa_1 - \frac{\pi}{t_{f2}} > 0$, $L^{'''} = \kappa_1 - \frac{\pi}{2t_{f2}}\big(1 + \cot(\frac{\pi t_{f1}}{2t_{f2}})\big) > 0$ and $\overline{L} = \min\{L^{''}, L^{'''}\} > 0$. According to Lemma 1, it is obtained that $\lim_{t\to t_{f2}^-} V_4 = 0$, which is equivalent to $\lim_{t\to t_{f2}^-} \Xi_2 x_2 = 0$ and $\lim_{t\to t_{f2}^-} \Xi_2^{(1)} x_1 = 0$. Because the condition $\Xi_2^{(1)} = \frac{\pi}{t_{f2}} \Xi_2 t g_2(t)$ is satisfied, it's easy to obtain that $\lim_{t\to t_{f2}^-} \Xi_2 x_1 = 0$. Those imply that the control input is bounded over $t \in [t_{f1}, t_{f2})$ with the control law (11).

In the time interval $D_2 : t \in [t_{f2}, \infty)$, the sliding mode surface and control law switch to the following forms

$$s = x_2 + k_2 x_1$$

$$u = -b^{-1}\big(\hat{\Delta} + k_1 s + k_2 x_2 + f + l\,\mathrm{sign}(s)\big)$$

where the term $\kappa_1 \Xi_2 x_1$ switches to $k_2 x_1$ and $\kappa_1 \Xi_2 x_2 + \kappa_1 \Xi_2^{(1)} x_1$ switches to $k_2 x_2$. Obviously, it is easy to obtain that $\lim_{t\to t_{f2}^-} \kappa_1 \Xi_2 x_1 = \lim_{t\to t_{f2}^+} k_2 x_1 = 0$ and $\lim_{t\to t_{f2}^-} \kappa_1 \Xi_2 x_2 + \kappa_1 \Xi_2^{(1)} x_1 = \lim_{t\to t_{f2}^+} k_2 x_2 = 0$.

For the time interval $D_2 : t \in [t_{f2}, \infty)$, the Lyapunov function candidate is also chosen as V_3, we readily obtain:

$$V_3(t_{f2}) = \lim_{t\to t_{f2}^-} V_3(t) = 0$$

$$\dot{V}_3 = -k_2 x_1^2 - k_2 x_2^2 \le 0, \qquad t \in [t_{f2}, \infty)$$

and it yields

$$0 \le V_3(t) \le V_3(t_{f2}) = 0, \qquad t \in [t_{f2}, \infty)$$

The conclusion remains valid over the time interval D_2, which completes the proof of point 2). It is obtained that system (1) is strong free-will arbitrary-time stable. In addition, above all imply that the control input is bounded over $t \in [0, \infty)$ with the control law (11). And this completes the proof of Theorem 2.

Remark 3 Compared with the traditional finite/fixed time control that based on fractional-power state feedback, by using the proposed prescribed finite-time control method, the convergence time of the system is a prescribed finite time, which don't depends on the initial state and design parameters and can be set in advance. The system states can be guaranteed to converge to the origin in the prescribed time firstly. Then, they can remain on the origin after the prescribed instant by switching the control law to another form. In addition, the switching process is a continuous transition. Compared with some existing prescribed-time controllers [18,19], this is a new attempt and is more conducive to practical application. Besides, the proposed control law is a novel SMC with prescribed finite-time convergence, which is rarely studied.

3 Application to partial IGC design

In this section, the proposed PFTESO-based PFTSMC method is applied to partial IGC design with two-loop controller structure [7].

3.1 Partial IGC model

Consider the nonlinear longitudinal model of a missile in pitch plane [2,7,30]:

$$\begin{bmatrix} \dot{\alpha} \\ \dot{V} \\ \dot{\theta} \\ \dot{q} \\ \dot{n}_L \end{bmatrix} = \begin{bmatrix} -\frac{K_f \rho V^2 C_x}{mV}\sin\alpha + \frac{K_f \rho V^2 C_z}{mV}\cos\alpha + q \\ \frac{K_f \rho V^2 C_x}{m}\cos\alpha + \frac{K_f \rho V^2 C_z}{m}\sin\alpha \\ q \\ \frac{K_m \bar{q}}{I_{yy}} C_m \\ -\frac{n_L}{Ta} + \frac{Vq}{Ta} \end{bmatrix} + \begin{bmatrix} 0 \\ 0 \\ 0 \\ \frac{K_m \bar{q}}{I_{yy}} C_m^{\delta_e} \\ 0 \end{bmatrix} \cdot \delta_e$$

where α, V, θ and q denote the angle of attack (AOA), velocity, pitch angle and pitch rate of missile. The missile is supposed to have its mass m, normal acceleration n_L and elevator deflection δ_e. $T_a = \frac{\alpha}{\dot{\gamma}_M} = V\left(\frac{m}{\bar{q}S}\right) \cdot \left(\frac{\partial C_L}{\partial \alpha}\right)^{-1}$ is the time constant of turning rate [1,7,30], with S being the missile reference surface, C_L being the coefficient of normal acceleration n_L. In addition, $\bar{q}$ is the dynamic pressure, and can be expressed as $\bar{q} = \frac{1}{2}\rho V^2$ with ρ being atmospheric density; I_{yy} is the moment of inertia around the pitch axis; $C_m^{\delta_e}$ is the coefficient of pitching moment with respect to δ_e; K_f and K_m are the constants determined by the missile geometry; moreover, the aerodynamic coefficients C_x, C_z and C_m are determined by affine functions [7].

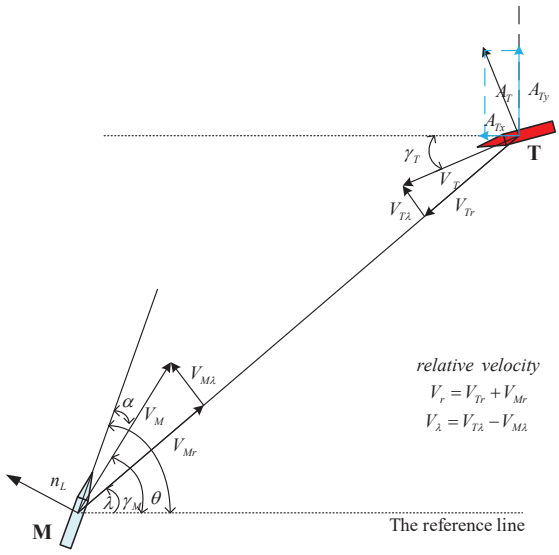

Fig. 2 Schematic diagram of relative motion of missile and target

Consider the interception problem within the perpendicular plane, Fig. 2 shows the schematic view of the two-dimensional (2-D) planar homing engagement geometry between an interceptor and a target. **M** denotes the missile and the target is denoted by **T**. γ_M and γ_T denote their flight path angles, respectively; the line of sight (LOS) angle and LOS distance are given by λ and r; V_M is represented as the velocity of missile; the target is supposed to have its velocity V_T and acceleration A_T, with A_{Tx}, A_{Ty} are the components of A_T along the $x-$axis and $y-$axis, respectively.

The planar missile-target engagement kinematics can be written as [1,7,30]:

$$\begin{cases} \dot{r} = V_r, \\ \dot{V}_r = V_\lambda^2/r + A_{Tr} - \sin(\lambda - \gamma_M)\, n_L \\ \dot{\lambda} = V_\lambda/r \\ \dot{V}_\lambda = -V_r V_\lambda/r + A_{T\lambda} - \cos(\lambda - \gamma_M)\, n_L \end{cases}$$

where $\dot{\lambda} = \omega_\lambda$ is the LOS rate; $V_\lambda = r\omega_\lambda$ is a component of relative velocity orthogonal to the LOS; V_r is the relative velocity along the LOS. Similarly, assuming r, V_r, λ, $\dot{\lambda}$ and $V_\lambda = r\dot{\lambda}$ are the state variables measured by radar [32]. Alternatively, A_{Tr} and $A_{T\lambda}$ are components of target acceleration along and orthogonal to LOS. Then the following Assumptions are introduced[1, 7]:

Assumption 2 Due to physical limitations, the target acceleration A_T and its first-order time derivative $\dot{A}_T$ are unknown, but bounded and continuous, i.e., $A_{T\lambda}$

is differentiable and $|A_{Tx}| \le A_{Tx}^{\max}$, $|A_{Ty}| \le A_{Ty}^{\max}$, $|A_{Tr}| \le A_{Tr}^{\max}$, $|A_{T\lambda}| \le A_{T\lambda}^{\max}$, $|\dot{A}_{T\lambda}| \le \dot{A}_{T\lambda}^{\max}$, where the positive scalars $A_{Tx}^{\max}$, $A_{Ty}^{\max}$, $A_{Tr}^{\max}$, $A_{T\lambda}^{\max}$ and $\dot{A}_{T\lambda}^{\max}$ are the unknown upper bound values.

Assumption 3 Due to physical limitations, the missile velocity V_M and the target velocity V_T are bounded, i.e., V_r and V_λ are bounded, satisfy $|V_r| \le V_r^{\max}$, $|V_\lambda| \le V_\lambda^{\max}$, and the positive scalars $V_r^{\max}$ and $V_\lambda^{\max}$ are the unknown upper bound values.

An effective hit-to-kill interception strategy can be achieved if the condition $V_\lambda \to c_0\sqrt{r}$ is satisfied [1], where $c_0 > 0$ is a given constant. Let $\sigma = V_\lambda - c_0\sqrt{r} \to 0$, then the interception strategy can be rewritten as $\sigma \to 0$; this command σ serves as the desired instruction signal of the interceptor control system, which can improve the robustness and accuracy of hit-to-kill interception [1,7].

Refer to the structure of partial IGC in [7], the partial integrated design method of control and guidance with two-loop structure is adopted. Therein, the model of outer loop can be obtained by differentiating σ until virtual control input q_c appears

$$\begin{cases} \dot{\sigma} = -\frac{V_\lambda V_r}{r} - \frac{c_0 V_r}{2\sqrt{r}} - \cos(\lambda - \gamma_M) n_L + A_{T\lambda} \\ \ddot{\sigma} = f_1 + b_1 q_c + \Delta \end{cases} \Rightarrow \begin{cases} \dot{\sigma}_1 = \sigma_2 \\ \dot{\sigma}_2 = f_1 + b_1 q_c + \Delta \end{cases} \tag{13}$$

where f_1 and b_1 are functions those are only related to the available variables, and their expressions could be found in [7]. On the contrary, Δ is related to the unknown target accelerations. Consider the inherent length of the target and the interceptor, we know that $r = 0$ will not achieve in real interception, and based on **Assumptions** 2 - 3, Δ can be regarded as the disturbance that satisfies $|\Delta| \le \Delta_{\max}$ and $|\dot{\Delta}| \le \dot{\Delta}_{\max}$, where $\Delta_{\max}$ and $\dot{\Delta}_{\max}$ are unknown and bounded positive constants.

Let $e = q_c - q$, differentiating it with respect to time once, it yields

$$\begin{cases} \dot{e}_1 = e_2 \\ \dot{e}_2 = f_2 + b_2 \delta_e \end{cases} \tag{14}$$

where $e_1 = \int_0^t e(\tau)d\tau$, $e_2 = e$; and f_2, b_2 are the known functions [7].

Control objective: In this study, it is expected that the partial IGC system can achieve stability in a prescribed finite time. It requires us to design a corresponding prescribed finite-time observer to estimate the unmeasured disturbance, and design corresponding prescribed finite-time control strategy to ensure that the system states can be stable in a prescribed finite time.

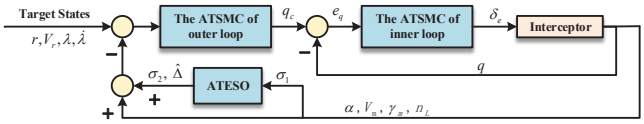

Fig. 3 The structure diagram of the prescribed finite-time convergent partial IGC system

The structure diagram of the prescribed finite-time convergent partial IGC system is shown in Fig. 3. The pitch rate command q_c is used as the virtual control input in the outer loop. The control objective of inner loop is to design a PFTSMC law for elevator deflection δ_e, so that the pitch rate q can track the reference signal q_c. As for outer loop, a novel PFTESO is proposed for estimating the disturbance Δ, and then PFTSMC law is designed for producing the command q_c to bring $\sigma \to 0$.

3.2 PFTESO-based PFTSMC Design for Partial IGC

According to Theorem 1, the disturbance Δ in outer loop can be estimated by the proposed PFTESO. And according to Theorem 2, the control inputs δ_e and q_c could be designed as follows to make e and σ prescribed finite-time stable.

$$\delta_e = \begin{cases} -b_2^{-1}\big(\kappa_{i1}\Xi_{i2}e_2 + \kappa_{i1}\Xi_{i2}^{(1)}e_1 + \kappa_{i2}\Xi_{i1}s_1 + f_2 \\ +l_i\,\mathrm{sign}(s_1)\big), t \in [0, t_{fi1}) \\ -b_2^{-1}\big(\kappa_{i1}\Xi_{i2}e_2 + \kappa_{i1}\Xi_{i2}^{(1)}e_1 + k_{i1}s_1 + f_2 \\ +l_i\,\mathrm{sign}(s_1)\big), t \in [t_{fi1}, t_{fi2}) \\ -b_2^{-1}\big(k_{i1}s_1 + k_{i2}e_2 + f_2 \\ +l_i\,\mathrm{sign}(s_1)\big), t \in [t_{fi2}, +\infty) \end{cases}$$

$$q_c = \begin{cases} -{b_1}^{-1}\big(\hat{\Delta} + \kappa_{o1}\Xi_{o2}\sigma_2 + \kappa_{o1}\Xi_{o2}^{(1)}\sigma_1 + \kappa_{o2}\Xi_{o1}s_2 \\ +f_1 + l_o\,\mathrm{sign}(s_2)\big), t \in [0, t_{fo1}) \\ -{b_1}^{-1}\big(\hat{\Delta} + \kappa_{o1}\Xi_{o2}\sigma_2 + \kappa_{o1}\Xi_{o2}^{(1)}\sigma_1 + k_{o1}s_2 \\ +f_1 + l_o\,\mathrm{sign}(s_2)\big), t \in [t_{fo1}, t_{fo2}) \\ -{b_1}^{-1}\big(\hat{\Delta} + k_{o2}\sigma_2 + k_{o1}s_2 \\ +f_1 + l_o\,\mathrm{sign}(s_2)\big), t \in [t_{fo2}, +\infty) \end{cases}$$

and the sliding manifolds are designed as follows:

$$s_1 = \begin{cases} e_2 + \kappa_{i1}\Xi_{i2}e_1, & t \in [0, t_{fi2}) \\ e_2 + k_{i2}e_1, & t \in [t_{fi2}, +\infty) \end{cases}$$

$$s_2 = \begin{cases} \sigma_2 + \kappa_{o1}\Xi_{o2}\sigma_1, & t \in [0, t_{fo2}) \\ \sigma_2 + k_{o2}\sigma_1, & t \in [t_{fo2}, +\infty) \end{cases}$$

Remark 4 Since the monotonically increasing function (2) will go to infinity as time tends to the prescribed time, it will cause some numerical simulation difficulties and obstacles. Similar to the practice in references [28,29], this problem can be alleviated by setting a smaller value of switch time $\overline{t}_{switch}$ than the prescribed convergence time $\overline{t}_f$ [17]. However, this approach can

only guarantee that the observation errors converge to the neighborhood of the origin as $t \to \overline{t}_{switch}$. If the selected $\overline{t}_{switch}$ is close enough to prescribed time $\overline{t}_f$, the convergence precision can be guaranteed. For the switched systems, according to Lyapunov stability theory, $\dot{V} \leq 0$ can be still maintained. Thus, the systems (5), (13) and (14) are still stable and the accuracy can be maintained simultaneously.

Remark 5 To weaken the effect of chattering, a saturation function sat$(\cdot)$ is often used to replace the sign function sign$(\cdot)$ [7,30], which can be expressed as

$$\text{sat}(x) = \begin{cases} \text{sign}(x), & |x| > \varepsilon \\ x/\varepsilon, & |x| \leq \varepsilon \end{cases}$$

where ε is the size of the boundary. By choosing an appropriate boundary value ε, the problem of frequent chattering can be alleviated on the premise of ensuring accuracy [30].

4 Simulation results

4.1 Validation of PFTESO

To show the effectiveness of the new PFTESO, the following second-order system is introduced as

$$\begin{cases} \dot{x}_1(t) = x_2(t) \\ \dot{x}_2(t) = d(t) \end{cases}$$

where $d = 100\cos(\frac{\pi}{3}t)$ needs to be observed, and the initial value of the state vector is set to be $[0,0]^T$. PFTESO for the aforementioned system is constructed as

$$\begin{cases} \varphi_1 = x_1 - z_1 \\ \dot{z}_1 = z_2 + \mathcal{T} l_1 \zeta \overline{\Xi} \varphi_1 + (1-\mathcal{T}) k_1 \Gamma^{\frac{1}{3}} \lceil \varphi_1 \rfloor^{\frac{2}{3}} \\ \dot{z}_2 = z_3 + \mathcal{T} l_2 \zeta^2 \overline{\Xi}^2 \varphi_1 + (1-\mathcal{T}) k_2 \Gamma^{\frac{2}{3}} \lceil \varphi_1 \rfloor^{\frac{1}{3}} \\ \dot{z}_3 = \mathcal{T} l_3 \zeta^3 \overline{\Xi}^3 \varphi_1 + (1-\mathcal{T}) k_3 \Gamma \lceil \varphi_1 \rfloor^0 \end{cases}$$

where the prescribed convergence time is selected as $\overline{t}_f = 0.5s$, $\zeta = 4$, $l_1 = 6$, $l_2 = 8$, $l_3 = 2$, $\Gamma = 120$, $k_3 = 130$, $k_1 = 3.34k_3^{\frac{1}{3}}$ and $k_2 = 5.3k_3^{\frac{2}{3}}$. In order to show the good observation performance of the proposed PFTESO, three kinds of ESO are chosen as:

1) Linear ESO [26]

$$\begin{cases} \dot{z}_1 = z_2 + \beta_1 \varphi_1 \\ \dot{z}_2 = z_3 + \beta_2 \varphi_1 \\ \dot{z}_3 = \beta_3 \varphi_1 \end{cases}$$

where the parameters are selected as $\beta_1 = 300$, $\beta_2 = 30000$, $\beta_3 = 1000000$.

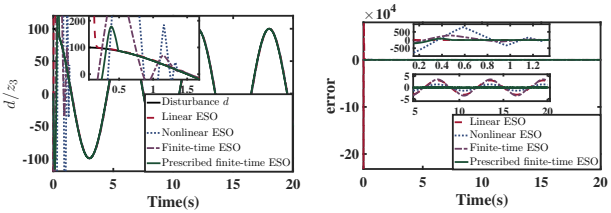

Fig. 4 Observation tracking curves and observation error curves for case 1

2) Nonlinear ESO [25]

$$\begin{cases} \dot{z}_1 = z_2 + \frac{\overline{k}_1}{r} \text{fal}\left(r^2(\varphi_1), \theta_1, 1\right) \\ \dot{z}_2 = z_3 + \overline{k}_2 \text{fal}\left(r^2(\varphi_1), \theta_2, 1\right) \\ \dot{z}_3 = \overline{k}_3 r \text{fal}\left(r^2(\varphi_1), \theta_3, 1\right) \end{cases}$$

where the nonlinear function fal(τ, θ, δ) is of the following form, and the parameters are selected as $\overline{k}_1 = 10$, $\overline{k}_2 = 20$, $\overline{k}_3 = 50$; $\theta_1 = 0.7$, $\theta_2 = 0.4$, $\theta_3 = 0.1$; r is a parameter that affects the accuracy of the observation, and is selected here as $r = 30$.

$$\text{fal}(\tau, \theta, \delta) = \begin{cases} \frac{\tau}{\delta^{1-\theta}}, & |\tau| \leq \delta \\ |\tau|^\theta \text{sign}(\tau), & |\tau| > \delta \end{cases}$$

3) Finite-time ESO [27]

$$\begin{cases} \dot{z}_1 = z_2 + \overline{\beta}_1 \varphi_1 \\ \dot{z}_2 = z_3 + \overline{\beta}_2 \lceil \varphi_1 \rfloor^{\gamma_1} \\ \dot{z}_3 = \overline{\beta}_3 \lceil \varphi_1 \rfloor^{\gamma_2} \end{cases}$$

where the parameters are selected as $\overline{\beta}_1 = 1$, $\overline{\beta}_2 = 300$, $\overline{\beta}_3 = 8000$; $\gamma_1 = 0.6$, $\gamma_2 = 0.4$. Besides, the initial values of the observers are all set to $[100, 5, 0]^T$. Then, the results of the comparison are shown in Fig. 4.

It can be seen from the Fig. 4 that the observation results of the four observers are all satisfactory. However, linear ESO in [26] requires high gain to improve observation accuracy, the peaking value problem may be serious and unacceptable. Even by introducing suitable nonlinear terms in nonlinear ESO [25] and finite-time ESO [27], the peaking value problem can be reduced to a certain extent, but the effect is limited. Since the properties of the function $\overline{\Xi}$ are those $\overline{\Xi}(0) = 1$ and $\overline{\Xi}(\overline{t}_f) = +\infty$, the initial gain of the proposed PFTESO is small, which can effectively alleviate the peaking value problem. The simulation results in the right part of Fig. 4 shows that the observation accuracy of PFTESO is much better than that of the other three observers.

In order to improve the observation accuracy of the other three observers, their parameters are increased as $\beta_1 = 3000$, $\beta_2 = 3000000$, $\beta_3 = 10^9$; $r = 200$; $\overline{\beta}_1 = 1000$, $\overline{\beta}_2 = 10000$, $\overline{\beta}_3 = 60000$. The error curves in Fig. 5 show that as the gains increase, the observation accuracy improves, but the peaking value problem

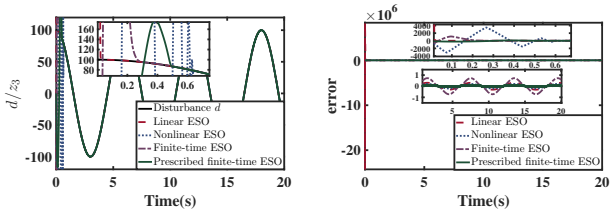

Fig. 5 Observation tracking curves and observation error curves for case 2

becomes more serious. Based on the above discussion, the designed PFTESO can not only greatly improve the observation accuracy, but also effectively reduce the peaking value problem.

4.2 Validation of prescribed finite-time control law

In this subsection, simulations are carried out to evaluate the control performance of the proposed control strategy in partial IGC design. The nonlinear 2-D engagement kinematics and interceptor model are applied in the simulations. The parameters of target and interceptor are given:

1) interceptor parameters: initial position $x_M(0) = 0$ m, $y_M(0) = 0$ m; initial velocity $V(0) = 800$ m/s;

2) target parameters: initial position $x_T(0) = 8000$ m, $y_T(0) = 8000$ m; initial velocity $V_{Tx}(0) = -100$ m/s; $V_{Ty}(0) = -200$ m/s.

More detailed dynamic parameters are the same as in [7]. The parameter of hit-to-kill interception strategy is selected as $c_0 = 0.01$; the parameters associated with the PFTSMC laws are given by

1) inner loop: $t_{fi1} = 1.2$ s, $t_{fi2} = 1.4$ s, $\kappa_{i1} = 5$, $\kappa_{i2} = 1.3$, $k_{i1} = 20$, $k_{i2} = 50$, $l_i = 1$;

2) outer loop: $t_{fo1} = 1.8$ s, $t_{f02} = 2.0$ s, $\kappa_{o1} = 13$, $\kappa_{o2} = 0.9$, $k_{o1} = 20$, $k_{o2} = 30$, $l_o = 1$;

3) The ESO parameters are tuned to be $\overline{t}_f = 1.6$ s, $l_1 = 6$, $l_2 = 8$, $l_3 = 1$, $\zeta = 4$, $\Gamma = 90$, $k_3 = 110$, $k_1 = 3.34k_3^{\frac{1}{3}}$ and $k_2 = 5.3k_3^{\frac{2}{3}}$.

To show the effectiveness of the proposed control strategy for a maneuvering target, the accelerations of the target are chosen as $A_{Tx} = 50\sin(0.4t)$ (m/s^2) and $A_{Ty} = 50\sin(0.8t)$ (m/s^2). And consider different sizes of the initial flight-path angle γ_{M0}: 1.485 rad, 1.085 rad, 0.785 rad, 0.485 rad and 0.185 rad, the simulation results are shown in Figs. 6 - 8 and Table 1.

The trajectories of missile and target are firstly shown in Fig. 6, and the flight time and miss distance of the interception for 5 cases can be found in Table 1. As it can be seen that the missile intercepts the target well in the cases of 5 different initial flight-path angles.

In addition, Fig. 7 shows the observation error curves of proposed PFTESO, which reveals that the observation errors converge to the origin within the prescribed time $\overline{t}_f = 1.6$ s. The observation errors can be maintained after switching, which guarantees the high observation accuracy. The conclusions claimed in Theorem 1 have been demonstrated.

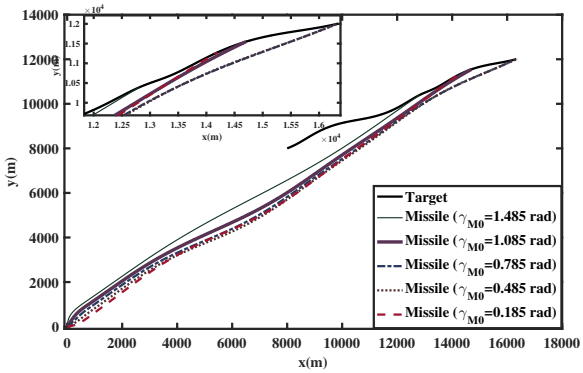

Fig. 6 Trajectories for 5 different initial flight-path angles

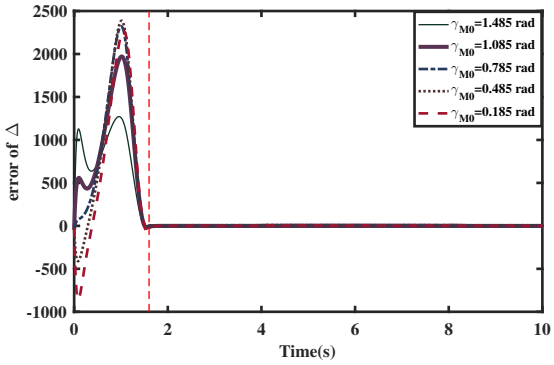

Fig. 7 Observation error curves for 5 cases

Table 1 The flight time and miss distance of the interception for 5 cases.

γ_{M0}(rad)	**Flight Time** (s)	**Miss distance** (m)
1.485	14.27	0.0268
1.085	21.36	0.0170
0.785	25.03	0.0109
0.485	25.08	0.0109
0.185	20.01	0.0098

To verify the correctness of Theorem 2, the simulation results of the inner loop state variables $e_{1,2}$, outer loop state variables $\sigma_{1,2}$ and sliding surfaces $s_{1,2}$ for 5 cases can be found in Fig. 8. It reveals that all these states can converge to the origin within the prescribed time, and can be maintained after switching. It indicates that the proposed control strategy provides good convergence performance for the system states and the convergence can be realized in the prescribed setting time. The correctness of Theorem 2 has been demonstrated. The curve of missile's AOA with 5 different

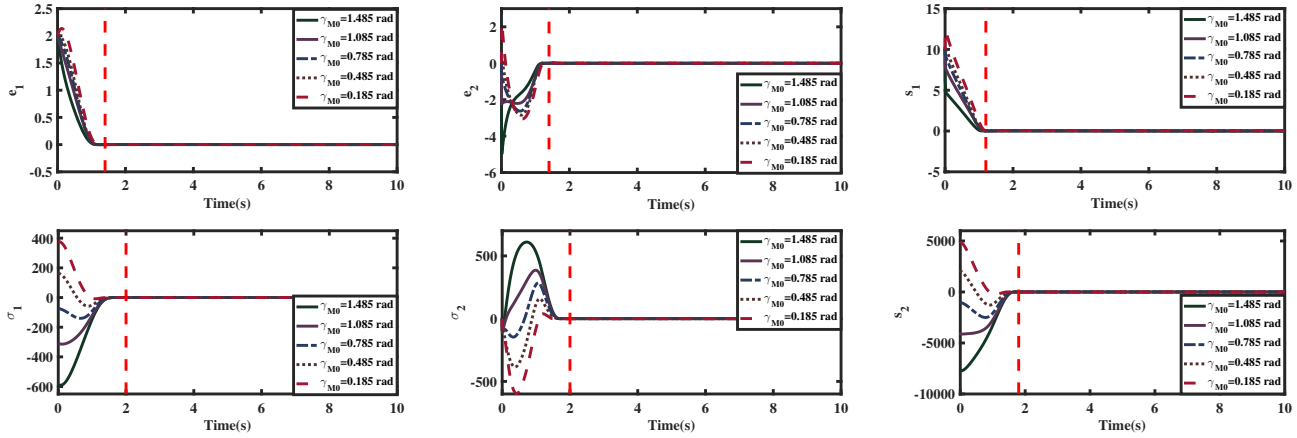

Fig. 8 The curves of $e_{1,2}$, s_1, $\sigma_{1,2}$ and s_2 for 5 cases

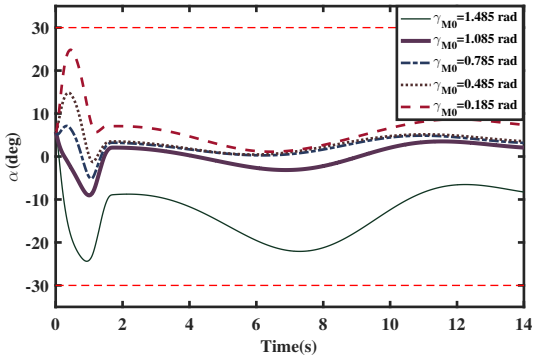

Fig. 9 Missile's angle of attack

initial flight-path angles γ_{M0} is given in Fig. 9. It illustrates that even in the two extreme initial conditions $\big(\gamma_{M0} = 1.485(\text{rad}) \text{ and } 0.185(\text{rad})\big)$, the missile's AOA is still within the desired range $[-30°, 30°]$, which means it is stable in the whole homing guidance process when target maneuvers persist.

4.3 Comparison results with the previous finite-time control law

In order to further demonstrate the better performance of proposed controller, it is compared with the adaptive finite-time sliding mode controller in [7]. The form of the finite-time control strategy is as follows

$$\begin{cases} \delta_e = b_2^{-1}\big(-f_2 - \lambda_2(e_1)e_2 - \widetilde{k}_1|s_1|^{\gamma_1}\text{sat}(s_1)\big) \\ s_1 = e_2 + \alpha_i|e_1| \quad (0<\alpha_i<1) \\ q_c = b_1^{-1}\big(-f_1 - \hat{\Delta}_{\max}\frac{\tau s_2}{|s_2|} - \lambda_1(\sigma_1)\sigma_2 - \widetilde{k}_2|s_2|^{\gamma_1}\text{sat}(s_2)\big) \\ s_2 = \sigma_2 + \alpha_o|\sigma_1| \quad (0<\alpha_o<1) \end{cases} \tag{15}$$

where $\hat{\Delta}_{\max}$ is determined by the following updating law:

$$\dot{\hat{\Delta}}_{\max} = \tau|s_2|$$

In order to make a fair comparison, all of initial conditions and simulation parameters are the same, and the accelerations of the maneuvering target are chosen the same as in the other subsections. The system response rates of the two controllers can be similar at the initial flight-path angles $\gamma_{M0} = 1.485$ rad by adjusting the parameters of the controller (15), which can be found in Fig. 11.

Fig. 10 shows the trajectories of missile and target at the initial flight-path angles $\gamma_{M0} = 1.485$ rad and $\gamma_{M0} = 0.185$ rad. It demonstrates that the interceptor can hit the maneuvering target well by using both two control strategies.

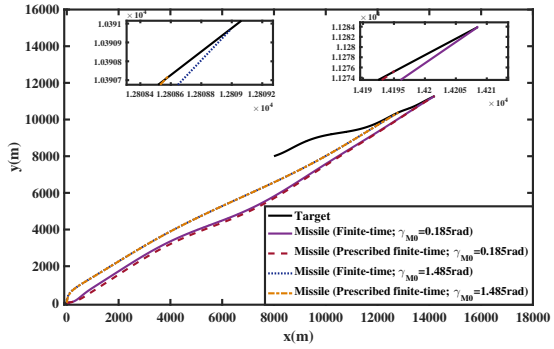

Fig. 10 Trajectories under the action of two control laws at the initial flight-path angle $\gamma_{M0} = 1.485$ rad and $\gamma_{M0} = 0.185$ rad

It should be noted that the $\hat{\Delta}_{\max}(0)$ in finite-time controller [7] needs to be large enough to compensate for the disturbance. Different to the adaptive estimation of disturbance, the total disturbance is extend-

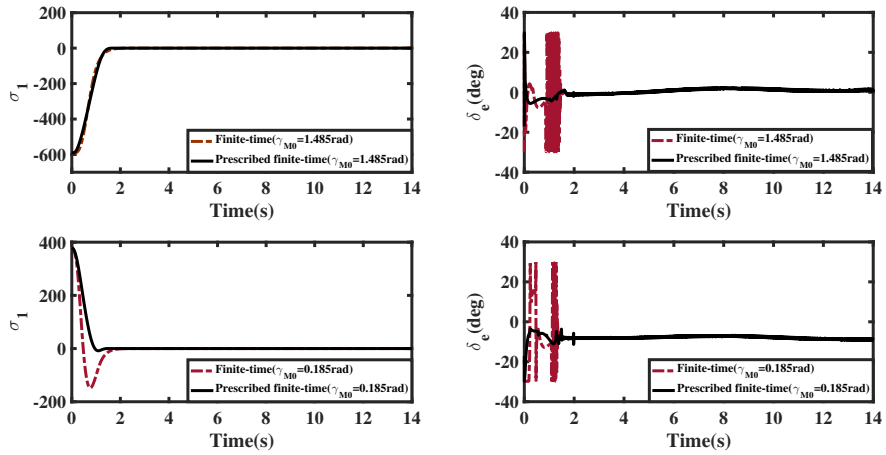

Fig. 11 The curves of state σ_1 and elevator deflection δ_e with the two control laws

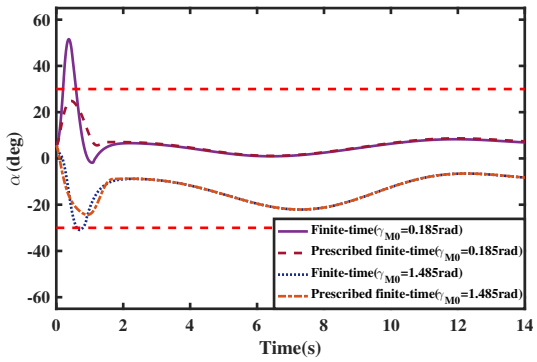

Fig. 12 Missile's angle of attack

ed as a state in the PFTESO for estimating. Noted that l_0 in this study is a small value compared with $\hat{\Delta}_{\max}$, thus the chattering and overestimation problem can be reduced. In addition, the simulation curves of state variable σ_1 and elevator deflection δ_e in these two cases can be found in Fig. 11. Obviously, the system response rates of the two controllers are similar at the initial flight-path angles $\gamma_{M0} = 1.485$ rad. However, at the initial flight-path angles $\gamma_{M0} = 0.185$ rad, the convergence time of the finite-time control becomes longer and the curve has obvious overshoot. The proposed control strategy ensures that the state can still converge within the prescribed convergence time with smaller overshoot. Besides, compared with the adaptive finite-time sliding mode controller in [7], it's easy to know the proposed controller can reduce the chattering effectively in Fig. 11. The reason is that the PFTESO resolves the overestimation of the robust term gain by estimating disturbance. Besides, Fig. 12 illustrates the curve of the AOA under the two control strategies, it shows that the AOA is in a reasonable region and the proposed control strategy is practical.

5 Conclusion

This paper aims at showing the viability and capability of the proposed PFTESO-based PFTSMC strategy for the second-order system with disturbance. Firstly, a new PFTESO has been constructed to approximate and compensate for disturbance, which can greatly improve the observation accuracy and effectively reduce the peaking value problem. Secondly, a novel PFTESO-based PFTSMC has been designed, so that the states and sliding mode variables of the system converge in a prescribed finite time, and can be maintained at the origin after the prescribed time. Thirdly, the PFTESO-based PFTSMC method has been successfully applied to partial IGC design to achieve prescribed finite-time stable. The stability is analyzed by using the Lyapunov stability theory. Finally, simulation results are conducted to show the effectiveness of the proposed new control strategy.

The simulation results reveal that: 1) compared with some existing ESOs, the proposed PFTESO has better observation performance. In addition, it can quickly estimate the disturbance and resolve the problem of the robust term gain overestimation, so that chattering phenomenon can be eliminated effectively; 2) the missile can intercept the maneuvering target well at different initial flight-path angles; 3) the system states, sliding mode variables and observation errors are well convergent in the prescribed time for different initial conditions. Therefore, the simulation results have verified that prescribed finite-time convergence stability could be guaranteed under the proposed control methodology, and the controller being employed can be successfully applied to partial IGC design.

Funding

This work was supported by the National Natural Science Foundation of China under Grant 61933014, the Aeronautical Science Foundation of China under Grant 201907048001 and Grant 20200001048001, and the Research Funds for the Engineering Research Center of Aircraft Autonomous Control Technology, Ministry of Education under Grant NJ2020004.

Compliance with ethical standards

Conflict of interest

All the authors in this manuscript declare that they have no conflict of interest.

Data availability statement

The data used to support the findings of this study are available from the corresponding author upon request.

References

1. Shtessel, Y.B., Shkolnikov, I.A., Levant, A.: Smooth second-order sliding modes: missile guidance application. Automatica. **43**(8), 1470–1476 (2007)
2. Shtessel, Y.B., Shkolnikov, I.A., Levant, A.: Guidance and control of missile interceptor using second-order sliding modes. IEEE Trans. Aerosp. Electron. Syst. **45**(1), 110–124 (2009)
3. Ni, J.K., Liu, L., Liu, C.X., Hu, X.Y., Shen, T.S.: Fixed-time dynamic surface high-order sliding mode control for chaotic oscillation in power system. Nonlinear Dyn. **86**, 401–420 (2016)
4. Lv, X.Y., Niu, Y.G., Song, J.: Finite-time boundedness of uncertain Hamiltonian systems via sliding mode control approach. Nonlinear Dyn. **104**, 497–507 (2021)
5. Shima, T., Idan, M., Golan, O.M.: Sliding-mode control for integrated missile autopilot guidance. J. Guid. Control Dyn.**29**(2), 250–260 (2006)
6. Zhao, Y., Liu, Y.F., Wen, G.H., Ren, W., Chen, G.R.:Edge-based finite-time protocol analysis with final consensus value and settling time estimations. IEEE Trans. Cybern. **50**(4), 1450–1459 (2020)
7. Wang, X.H., Wang, J.Z.: Partial integrated missile guidance and control with finite time convergence. J. Guid. Control Dyn. **36**(5), 1399–1409 (2013)
8. Song, H.T., Zhang, T.: Fast robust integrated guidance and control design of interceptors. IEEE Trans. Control Syst. Technol. **24**(1), 349–356 (2016)
9. Tian, B.L., Lu, H.C., Zuo, Z.Y., Wang, H.: Fixed-time stabilization of high-order integrator systems with mismatched disturbances. Nonlinear Dyn. **94**, 2889–2899 (2018)
10. Polyakov, A.: Nonlinear feedback design for fixed-time stabilization of linear control systems. IEEE Trans. Autom. Control. **57**(8), 2106–2110 (2012)
11. Meng, D.Y., Zuo, Z.Y.: Signed-average consensus for networks of agents: a nonlinear fixed-time convergence protocol. Nonlinear Dyn. **85**, 155–165 (2016)
12. Huang, Y., Jia, Y.M.: Fixed-time consensus tracking control of second-order multi-agent systems with inherent nonlinear dynamics via output feedback. Nonlinear Dyn. **91**, 1289–1306 (2018)
13. Ni, J.K., Tang, Y., Shi, P.: A new fixed-time consensus tracking approach for second-order multiagent systems under directed communication topology. In: IEEE Trans. Syst. Man. Cybern. Syst. https://doi.org/10.1109/TSMC.2019.2915562 (2019)
14. Chang, S.P., Wang, Y.J., Zuo, Z.Q.: Fixed-time active disturbance rejection control and its application to wheeled mobile robots. In: IEEE Trans. Syst. Man. Cybern. Syst. https://doi.org/10.1109/TSMC.2020.2966077 (2020)
15. Wang, Y.J., Song, Y.D., Hill, D.J., Krstic, M.: Prescribed-time consensus and containment control of networked multiagent systems. IEEE Trans. Cybern. **49**(4), 1138–1147 (2019)
16. Zhao, Y., Liu, Y.F., Wen, G.H., Ren, W., Chen, G.R.: Designing distributed specified-time consensus protocols for linear multiagent systems over directed graphs. IEEE Trans. Autom. Control. **64**(7), 2945–2952 (2019)
17. Guo, G., Gao, Z.Y., Dong, K.: Prescribed-time formation control of surface vessels with asymmetric constraints on LOS range and bearing angles. In: Nonlinear Dyn. https://doi.org/10.1007/s11071-021-06462-8 (2021)
18. Song, Y.D., Wang, Y.J., Holloway, J., Krstic, M.: Time-varying feedback for robust regulation of normal-form nonlinear systems in prescribed finite time. Automatica. **83**, 243–251 (2017)
19. Song, Y.D., Wang, Y.J., Krstic, M.: Time-varying feedback for stabilization in prescribed finite time. Int. J. Robust Nonlin. Control. **29**(3), 618–633 (2018)
20. Pal, A.K., Kamal, S., Nagar, S.K., Bandyopadhyay, B., Fridman, L.: Design of controllers with arbitrary convergence time. Automatica. **112**, 1–8 (2020)
21. Chen, W.H., Yang, J., Guo, L., Li, S.H.: Disturbance-observer-based control and related methods - an overview. IEEE Trans. Ind. Electron. **63**(2), 1083–1095 (2016)
22. Cristofaro, A., Johansen, T.A.: Fault tolerant control allocation using unknown input observers. Automatica. **50**(7), 1891–1897 (2014)
23. Dong, L.W., Wei, X.J., Hu, X., Zhang, H.F., Han, J.: Disturbance observer-based elegant anti-disturbance saturation control for a class of stochastic systems. Int. J. Control. **93**(12), 2859–2871 (2020)
24. Han, J.Q.: From PID to active disturbance rejection control. IEEE Trans. Ind. Electron. **56**(3), 900–906 (2009)
25. Zhao, Z.L., Guo, B.Z., A nonlinear extended state observer based on fractional power functions. Automatica. **81**, 286–296 (2017)
26. Liu, P., Xue, W.C., Chen, S., Huang, Y., Sun, Z.D.: An integrated solution to ACMM problem of spacecraft with inertia uncertainty. Int. J. Robust Nonlin. Control. **28**(17), 5575–5589 (2018)
27. Sun, G.F., Ren, X., Chen, Q., Li, D.W.: A modified dynamic surface approach for control of nonlinear systems with unknown input dead zone. Int. J. Robust Nonlin. Control. **25**(8), 1145–1167 (2015)
28. Holloway, J., Krstic, M.: Prescribed-time observers for linear systems in observer canonical form. IEEE Trans. Autom. Control. **64**(9), 3905–3912 (2019)
29. Chang, L., Han, Q.L., Ge, X.H., Zhang, C.H., Zhang, X.F.: On designing distributed prescribed finite-time observers for strict-feedback nonlinear systems. In: IEEE

Trans. Cybern.
https://doi.org/10.1109/TCYB.2019.2951067 (2019)
30. Ji, Y., Lin, D.F., Pei, P., Shi, X.W., Wang, W.: Robust partial integrated guidance and control approaches for maneuvering targets. Int. J. Robust Nonlin. Control. **29**(18), 6522–6541 (2019)
31. Yan, H., Tan, S.P., Xie, Y.S.: Integrated translational and rotational control for the final approach phase of rendezvous and docking. Asian. J. Control. **20**(5), 1967–1978 (2018)
32. Yan, H., Ji, H.B.: Integrated guidance and control for dual-control missiles based on small-gain theorem. Automatica. **48**(10), 2686–2692 (2012)
33. Zhang, C., Wu, Y.J.: Non-singular terminal dynamic surface control based integrated guidance and control design and simulation. ISA Trans. **63**, 112–120 (2016)
34. Menon, P.K., Sweriduk, G.D., Ohlmeyer, E.J., Malyevac, D.S.: Integrated guidance and control of moving mass actuated kinetic warheads. J. Guid. Control Dyn. **27**(1), 118–126 (2004)
35. Yan, H., Wang, X.H., Yu, B.F., Ji, H.B.: Adaptive integrated guidance and control based on backstepping and input-to-state stability. Asian. J. Control. **16**(2), 602–608 (2014)
36. Zhang, Y., Tang, S., Guo, J.: Adaptive terminal angle constraint interception against maneuvering targets with fast fixed-time convergence. Int. J. Robust Nonlin. Control. **28**, 2996–3014 (2018)
37. Cruz-Zavala, E., Moreno, J.A.: Levant's arbitrary-order exact differentiator: a Lyapunov approach. IEEE Trans. Autom. Control. **64**(7), 3034–3039 (2019)